International Journal of Mechanical Sciences 85 (2014) 104–109

Contents lists available at ScienceDirect

International Journal of Mechanical Sciences

journal homepage: www.elsevier.com/locate/ijmecsci

Effect of contact angle on contact morphology and Vickers hardness measurement in instrumented indentation testing

Seung-Kyun Kang [a], Young-Cheon Kim [b], Jin-Woo Lee [c], Dongil Kwon [c], Ju-Young Kim [b,d,*]

[a] Department of Materials Science and Engineering, Frederick Seitz Materials Research Laboratory, University of Illinois at Urbana-Champaign, Urbana, IL 61801, USA
[b] School of Materials Science and Engineering, UNIST (Ulsan National Institute of Science and Technology), Ulsan 689-798, Republic of Korea
[c] Department of Materials Science and Engineering, Seoul National University, Seoul 151-744, Republic of Korea
[d] KIST-UNIST Ulsan Center for Convergent Materials, UNIST (Ulsan National Institute of Science and Technology), Ulsan 689-798, Republic of Korea

ARTICLE INFO

Article history:
Received 25 December 2013
Received in revised form
28 April 2014
Accepted 2 May 2014
Available online 20 May 2014

Keywords:
Contact angle
Contact morphology
Vickers hardness
Scaling relation
Instrumented indentation

ABSTRACT

We derive a general contact-depth function for the Vickers indenter by modifying a scaling relation between yield strain and indentation depth ratio, which is comprised of indenter angle, plastic constraint factor, and indentation depth ratio. The validity of this function is demonstrated by using various indenters of different angles. A method for calibrating the actual contact area of an imperfectly shaped Vickers indenter is suggested that yields a better evaluation of Vickers hardness in the instrumented indentation test.

1. Introduction

Understanding contact morphology is a fundamental issue in instrumented indentation testing. While Hertz's elastic contact solution has been generally used for various indenter geometries, plastic deformation underneath an indenter is not fully described by an analytical solution. Among suggested plasticity models in indentation, Johnson's expanding-cavity model is among the most commonly used [1]. Johnson extended Hill's spherical cavity model [1] to indentation contact problems by assuming a hemispherical cavity field underneath the indenter, which provided a good approximation to the stress–strain field under an indenter. However, it assumes conservation conditions, i.e. that the penetrated volume is the same as the expanding cavity volume; thus it does not allow for the effect of stress flow in inducing plastic pileup around the indenter. Describing material pileup around the indenter with simple analytic methods only is challenging, so much work has been performed using parametric analysis or/and computational simulation, generally finite element analysis (FEA) [2–13].

Cheng and Cheng suggested parametric analysis using FEA and proposed dominant instrumented indentation parameters determining material pileup to be (1) yield strain (ratio of yield strength to elastic modulus, σ_y/E), (2) indenter half-angle θ as described in Figs. 1, and (3) the strain-hardening exponent n. The average strain under the indenter is a constant regardless of indentation depth for a sharp geometrically self-similar indenter, and thus when the total strain is fixed for sharp indenter, the amount of plastic strain decreases as the yield strain increases. For a sharp indenter, the smaller θ induces higher total strain in materials so there may be plenty of room for greater plastic strain. The effect of the strain-hardening exponent n on materials pileup can be explained by the relative ease of propagating deformation to the undeformed zone; a higher strain-hardening exponent means that the strain-hardened deformed region becomes much harder than the neighboring undeformed region, resulting in less material pileup due to easier plastic flow [16–17].

We found that the yield strain is a primary factor determining material pileup among yield strain and strain-hardening exponent in Vickers indentations for 24 metallic materials [16]. We defined a contact-depth function f as

$$f = \frac{h_c}{h_{max}} = \frac{h_{max} - h_d + h_p}{h_{max}}, \quad (1)$$

where h_c is the contact depth that reflects elastic deflection h_d and plastic pileup h_p and h_{max} is the maximum indentation depth from the initial surface, as described in Fig. 1 (It is noteworthy that

* Corresponding author at: UNIST (Ulsan National Institute of Science and Technology), School of Materials Science and Engineering, Ulsan 689-798, Republic of Korea.
E-mail address: juyoung@unist.ac.kr (J.-Y. Kim).

http://dx.doi.org/10.1016/j.ijmecsci.2014.05.002
0020-7403/

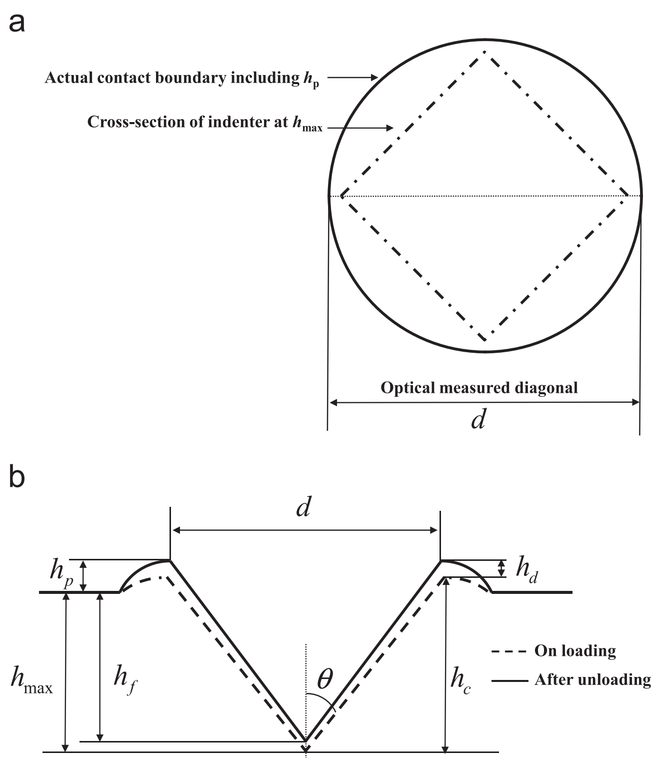

Fig. 1. Contact morphology of Vickers indentation: (a) top side view and (b) cross-sectional view.

although the actual pileup height is identical during unloading, this pileup height seems to increase due to elastic recovery of elastic deflection.) [18–21]. Experimental results show a linear relation between contact-depth function f and the inverse of the yield strain [16]:

$$f = a'\left(\frac{\sigma_y}{E_r}\right)^{-1} + b', \tag{2}$$

where a' and b' are constants, σ_y is the yield strength, and E_r is the reduced elastic modulus in instrumented indentation [19]. By the simple approximation that $H=\psi\sigma_y$, where H is the hardness and ψ is the plastic constraint factor, the yield strain can be replaced by the ratio of hardness to reduced elastic modulus H/E_r [16]. The scaling indentation relation between ratio of hardness to reduced elastic modulus H/E_r and elastic indentation energy ratio $W_{elastic}/W_{total}$, where $W_{elastic}$ is elastically stored work and W_{total} is total work induced during indentation, was used to evaluate the contact-depth function using indentation parameters only. Finally, the contact-depth function for projected area is determined from the maximum indentation depth and final indentation depth (h_f) as [16,17]

$$f = 1.06 \times 10^{-2}\frac{h_{max}}{h_{max}-h_f} + 1.00. \tag{3}$$

The contact-depth function for Vickers indenter f_V is determined by a similar derivation as

$$f_V = \frac{h_c^V}{h_{max}} = 9.90 \times 10^{-3}\frac{h_{max}}{h_{max}-h_f} + 1.00, \tag{4}$$

where h_c^V is the contact depth at the edge of the residual impression in Vickers indentation [16,17]. Eqs. (3) and (4) show that f and f_V are described by the ratio of indentation depths. Here the definitions of contact area and hence hardness differ in instrumented indentation and Vickers indentation. Hardness in instrumented indentation (H) uses the projected area as the nominal area; however, Vickers hardness (HV) uses the surface area of the Vickers indenter and calculates the area from the corner-to-corner length only. The conventional Vickers hardness is widely used for its simplicity, but in this paper, the derivation is on the basis of hardness in instrumented indentation so as to consider the pileup effects.

Here we suggest a theoretical analysis for the contact-depth function by investigating a scaling relation between yield strain and indentation depth ratio for the actual contact depth in Vickers indentation. We investigate the effects of material properties and sharp indenter angles on materials pileup. By combining theoretical analysis and experimental results, including the effects of material properties and sharp indenter angle on material pileup, we propose a novel way to determine contact-depth function and Vickers hardness.

2. Material and experimental details

Twenty-five metallic specimens (carbon steels – S20, S45C, SCM21, SCM4, SKD61, SKS3, SUJ2, API X70, API X100; stainless steels – SUS303F, SUS310S, SUS316L, SUS403, SUS410, SUS420J2; Ni alloy – Inconel 600; Al alloys – Al6061, Al7075; copper alloys – C1010, C5101, C62400; Ti alloys – Ti-10V–2Fe–3Al, Ti–7Al–4Mo) were prepared and polished gently with 1 μm diamond powder. Instrumented indentation testing was performed with an AIS System (FRONTICS, Korea) with force resolution 55 mN and displacement resolution 100 nm; three different four-sided pyramidal indenters with half-angles of 56.5°, 68.0°, and 75.8° were used. The indentation tests were performed with maximum indentation depth 80 μm at constant displacement rate 0.3 mm/min. The instruments were calibrated by the standard calibration procedure [22]. Residual indentation impressions were optically measured to evaluate contact depth from real contact area (A_c). The contact depth and contact area have the following geometrical relationship depending on the indenter half-angle for a pyramidal indenter:

$$h_c = \frac{\sqrt{A_c}}{2\ \tan\ \theta} \tag{5}$$

for a Vickers indenter, $\theta=68°$. The hardness in instrumented indentation, defined as P/A_c, is measured by the maximum load of instrumented indentation and the contact area as found by optical microscopy. The reduced elastic modulus was calculated as $\sqrt{\pi}S/2\sqrt{A_c}$, where S is the initial unloading slope measured from the unloading curve of instrumented indentation. The yield strength was measured by tension testing with cylindrical specimens of 25 mm length and 6 mm diameter.

We prepared standard hardness blocks of Vickers hardness 150, 200, 300 and 500 (Yamamoto Scientific Tool Laboratory Co., Ltd. Chiba, Japan) respectively, and three different commercial Vickers indenters (A.L.M.T. Co. Tokyo, Japan) to calibrate the contact-depth function depending on the geometrical imperfection of the indenters. Indentation was performed on standard hardness blocks for three different Vickers indenters and with maximum indentation depth of 80 μm. The diagonal lengths of residual indentation impressions d were measured by an optical microscope. Using the following relation in Vickers hardness (HV), we can derive h_c^V from d or HV by

$$HV = 1.8544P/d^2, \tag{6}$$

$$h_c^V = d/7, \tag{7}$$

where P is the maximum indentation load.

3. Theoretical Modeling

From the fundamental relation between yield strain and pileup, the yield strain has been approximated by indentation depth. The most important approximation was performed using the scaling relation:

$$k\frac{H}{E_r}=\frac{W_{elastic}}{W_{total}}, \tag{8}$$

where k is generally taken as 5. Malzbender [8] has given an analytical solution using loading and unloading curves, and Cheng et al. [2,14,15] have proven that relation through dimensionless FEA analysis. However, Malzbender's approximation considers only elastic deflection, not the real contact depth including pileup, so we need to use the real contact-depth function to estimate an accurate solution, especially for metallic materials.

The indentation loading curve can be derived as follows assuming hardness to be constant regardless of indentation depth (note that here we do not consider the indentation size effect (ISE) because the indentation depth is 80 μm, where ISE is believed negligible):

$$H=\frac{P}{A_c}=\frac{P}{24.5h_c^2}, \tag{9}$$

$$P=24.5H\cdot h_c^2=24.5H\cdot f^2\cdot h^2 \tag{10}$$

where h is the indentation depth. The total work during indentation can be derived from the loading curve as

$$W_{total}=\int_0^{h_{max}} P\,dh=\int_0^{h_{max}} 24.5H\cdot f^2\cdot h^2\,dh=\frac{24.5}{3}H\cdot f^2\cdot h_{max}^3. \tag{11}$$

The unloading curve and elastic contact energy can be defined as

$$P=\frac{2\tan\theta}{\pi}E_r(h-h_f)^2, \tag{12}$$

$$W_{elastic}=\int_{h_f}^{h_{max}}\frac{2\tan\theta}{\pi}E_r(h-h_f)^2dh=\frac{2\tan\theta}{3\pi}E_r(h_{max}-h_f)^3. \tag{13}$$

Combining Eqs. (11) and (13) yields

$$\frac{W_{elastic}}{W_{total}}=\frac{2\tan\theta}{24.5\pi}\frac{E_r}{H}\frac{1}{f^2}\left(\frac{h_{max}-h_f}{h_{max}}\right)^3 \tag{14}$$

The ratio of the indentation works ($W_{elastic}/W_{total}$) can be approximated by the ratio of indentation depths ($(h_{max}-h_f)/h_{max}$), as shown in Fig. 2 [23]. By using this approximation to Eq. (14), we obtain:

$$\frac{W_{elastic}}{W_{total}}=\frac{h_{max}-h_f}{h_{max}}=\frac{2\tan\theta}{24.5\pi}\frac{E_r}{H}\frac{1}{f^2}\left(\frac{h_{max}-h_f}{h_{max}}\right)^3, \tag{15}$$

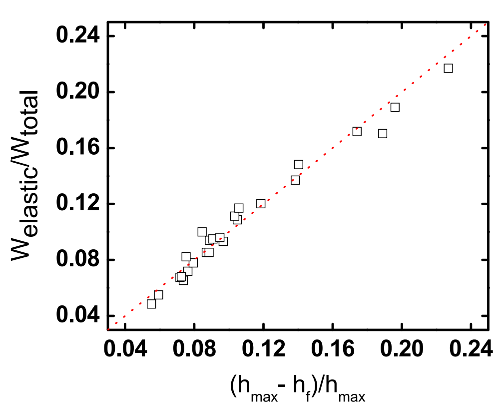

Fig. 2. Linear approximation of indentation works in indentation depths.

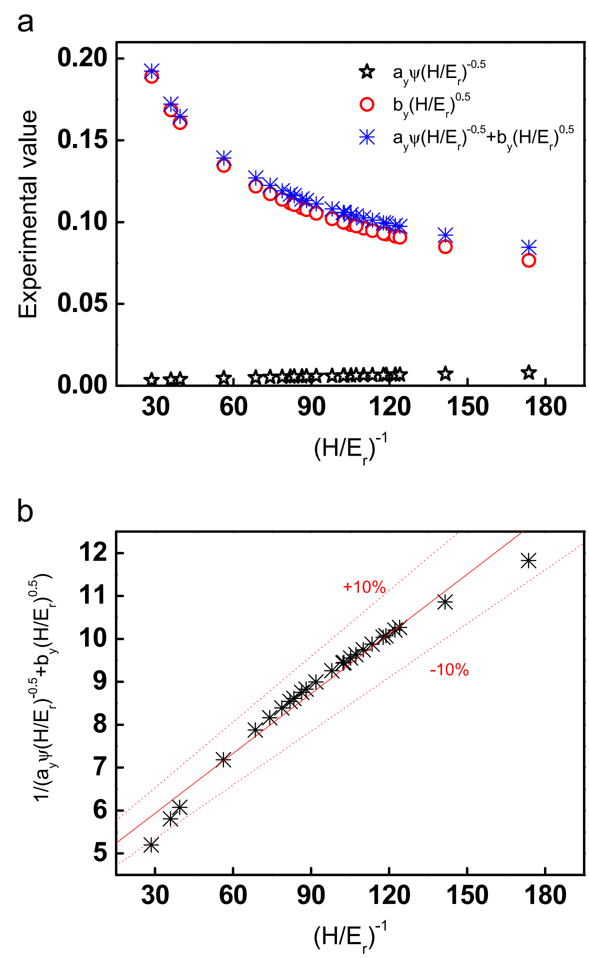

Fig. 3. Statistical approximation of functions of H/E_r.

$$\frac{h_{max}}{h_{max}-h_f}=\sqrt{\frac{2\tan\theta}{24.5\pi}}\sqrt{\frac{E_r}{H}\frac{1}{f}}. \tag{16}$$

Here the contact-depth function f for a Vickers indenter is represented by the yield strain with Eq. (3) and the yield strain can be expressed in terms of the hardness and plastic constraint factor, so that Eq. (16) can be written as

$$\frac{h_{max}}{h_{max}-h_f}=\sqrt{\frac{2\tan\theta}{24.5\pi}}\sqrt{\frac{E_r}{H}\frac{1}{f}}=\sqrt{\frac{2\tan\theta}{24.5\pi}\frac{1}{a'\psi(H/E_r)^{-0.5}+b'(H/E_r)^{0.5}}} \tag{17}$$

In this modified scaling relation, the indentation depth ratio is expressed by the square root of H/E_r. To simplify this relation, we check the relation between $a'\psi(H/E_r)^{-0.5}+b(H/E_r)^{0.5}$ and $(H/E_r)^{-1}$. Fig. 3a shows the relative values contributing to the total value depending on $(H/E_r)^{-1}$. The second term is dominant; indeed, it almost completely determines the total value. Fig. 3b shows that $(a'\psi(H/E_r)^{-0.5}+b'(H/E_r)^{0.5})^{-1}$ can be approximated as a linear relation with $(H/E_r)^{-1}$. We rewrite Eq. (17) as (18) by defining new constants a'', b'', and by rearrangement we can obtain Eq. (19):

$$\frac{h_{max}}{h_{max}-h_f}=\sqrt{\frac{2\tan\theta}{24.5\pi}}\sqrt{\frac{E_r}{H}\frac{1}{f}}\approx\sqrt{\frac{2\tan\theta}{24.5\pi}(a''(H/E_r)^{-1}+b'')}, \tag{18}$$

$$(H/E)^{-1}=\frac{a'''}{\sqrt{\tan\theta}}\frac{h_{max}}{h_{max}-h_f}+b''', \tag{19}$$

where a''' and b''' are also constants (note that b''' is negative). Combining Eqs. (2) and (19) yields

$$\begin{aligned} f &= a'(\sigma_y/E)^{-1} + b' = a'\psi(H/E)^{-1} + b' \\ &= a'\psi\left(\frac{a''}{\sqrt{\tan\,\theta}}\frac{h_{max}}{h_{max}-h_f} + b''\right) + b' \\ &= a\frac{\psi}{\sqrt{\tan\,\theta}}\frac{h_{max}}{h_{max}-h_f} + b \end{aligned} \tag{20}$$

in agreement with previous experimental work [16,17]. We can now analyze the theoretical meaning of each parameter.

4. Discussion

4.1. Contact angle effects

We investigate effects of indenter half-angle on relation between yield strain and plastic pileup. Fig. 4 shows the relation between contact-depth function and inverse of yield strain for three different indenters. The sharper indenter with higher indenter half-angle tends to induce less pileup. Mathematically, contact-depth functions for indenters with indenter half-angles of 56.5° and 75.8° are within $\pm$10% of the linear function fitted to experimental data obtained by the Vickers indenter.

Fig. 5 shows the relation between the contact-depth function and indentation depth ratio for three different indenters. The slopes in Fig. 5 are 0.0036, 0.0099, and 0.0111 and the y-axis intercepts are 1.0484, 0.9967, and 0.9266 for indenter angles of 56.5°, 68.0°, and 75.8° respectively (Table 1). During derivation of Eq. (20), the other equations prior to Eq. (20) are valid even if the indenter angle is different. From Eq. (20) and the deviation in yield strain and contact-depth function f, we can explain trends in the contact-depth functions for different indenter angles as shown in Fig. 5. In Eq. (20), the slope depends on the inverse of the square root of the tangential contact angle, so a relation proportional to

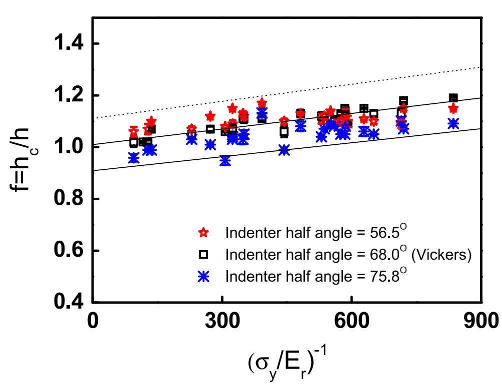

Fig. 4. Effects of indenting angle on the relation between yield strain and contact-depth function. Straight line is fitted to Vickers indenter and dotted lines are $\pm$10% deviation.

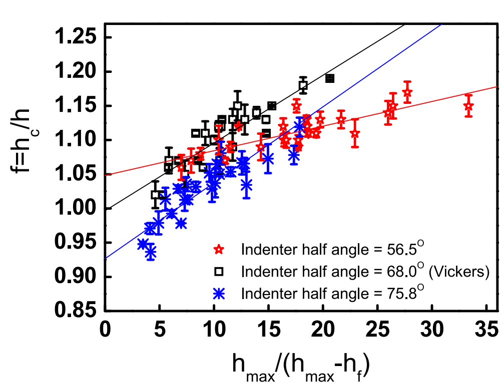

Fig. 5. Contact-depth function for indenters of three different angles.

Table 1
The constant of linear relation between indentation depths and contact depth function for three different angled indenters.

Half-angle of indenter (deg)	$a\frac{\psi}{\sqrt{\tan\,\theta}}$	b
56.5	0.0036	1.0484
68	0.0099	0.9967
75.8	0.0111	0.9266

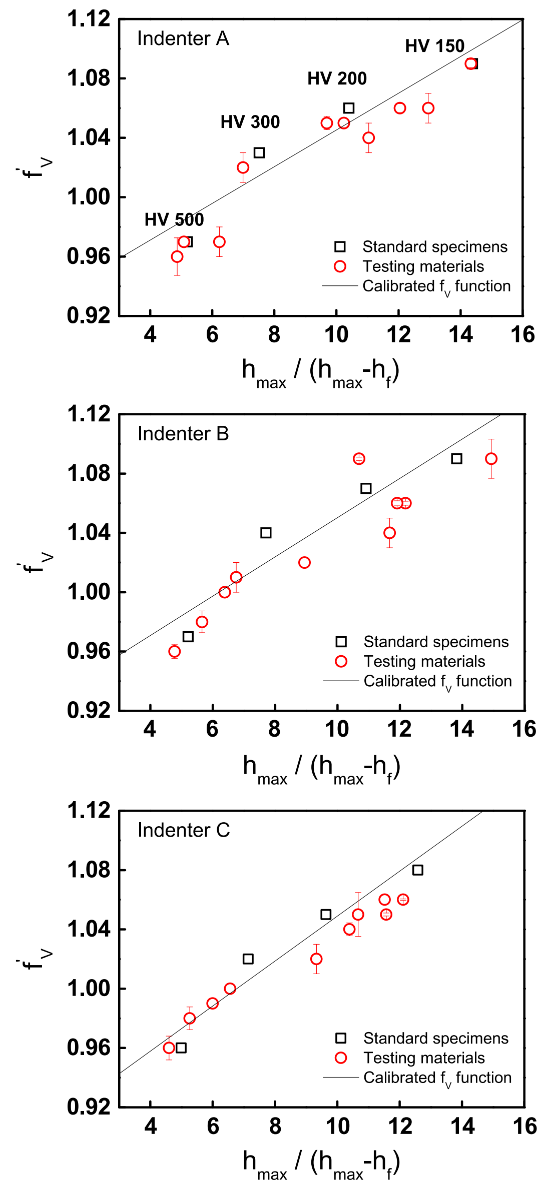

Fig. 6. Contact-depth functions of three commercial Vickers indenters derived by standard hardness blocks comparing with those for testing metals.

indenting angle can be expected. On the other hand, the y-axis intercept b is derived from b', which is inversely proportional to the indenter angle. These relations explain the increase in slope a and decrease in y-axis intercept b as the indenter angle increases.

4.2. Evaluation of Vickers hardness

Using Eq. (20), we can derive a simplified approach to evaluate the contact-depth equation including the indenter shape calibration. Even when the indenter angle changes, the linear relation

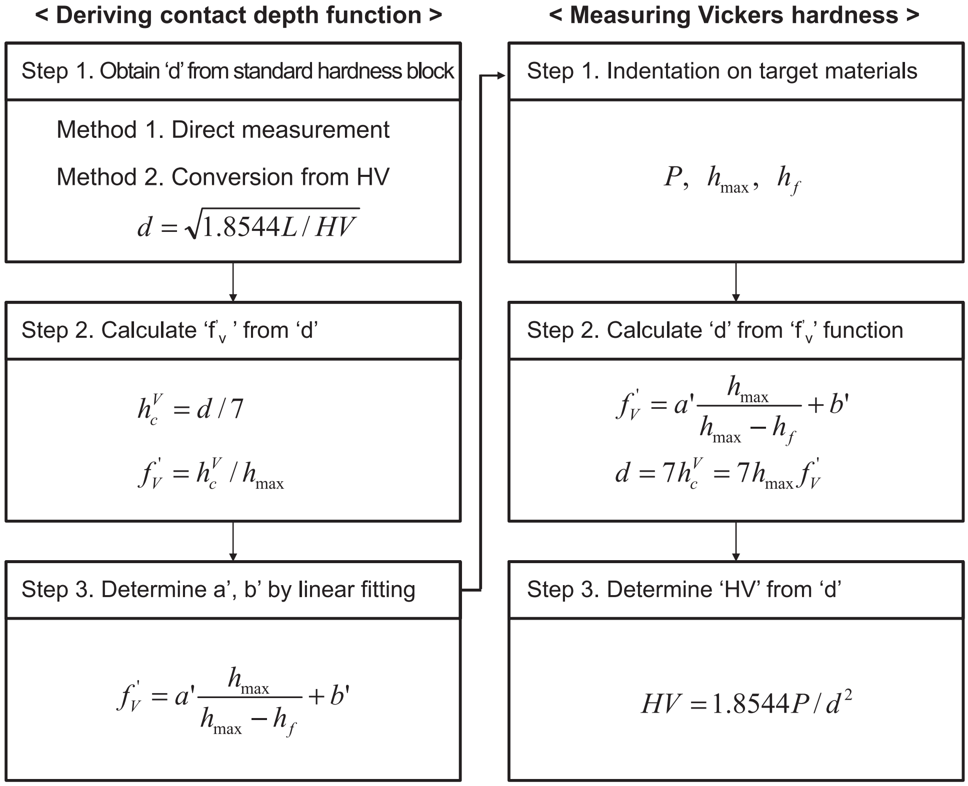

Fig. 7. Algorithms determining contact-depth function and conventional Vickers hardness experimentally by correcting imperfect geometry of Vickers indenter.

between contact-depth function and yield strain or indentation depth ratio is still valid. This implies that the indenter angle can be estimated from a linear approximation of the contact-depth function and indentation depth ratio for a sharp indenter with any indenter half-angle. The calibration for a slightly misfit orientation of indenter is far more critical in Vickers hardness derived by instrumented indentation than in the conventional Vickers hardness measurement, where the size of residual indentation impression is measured optically. With a misfit of $\pm 0.5^\circ$ in indenter angle, the change in hardness values is acceptable [24]; however, the contact area or diagonal length calculated from the contact depth using Eqs. (5) or (7) has crucial errors because it depends on the indenter angle as a tangential function. Thus, the contact area calculated from the indentation depth can make a great difference in the real contact area and should be calibrated. If we obtain some sets of data for f_V and $h_{max}/(h_{max}-h_f)$, we can determine a, b, and contact-depth function for accurate Vickers hardness. To obtain f_V, we first need to know d. We have two ways to obtain d: by using standard hardness blocks, from which the diagonal length can be converted, or by measuring it by the optical microscope. After obtaining d, f_V is derived from Eq. (7), and a and b in the contact-depth function can be determined by linear fit of f_V and $h_{max}/(h_{max}-h_f)$.

Fig. 6 shows the relation between f_V and $h_{max}/(h_{max}-h_f)$ for standard hardness blocks (where d is converted from the hardness number) and the linear function fitted to the experimental data. Fig. 6 also shows that this linear function well described the contact depth behavior of example alloys measured by different Vickers indenters, which imply that the contact depth function can be derived from the linear function generated by standard specimens. Here we need to note that f_V derived by Eq. (7) is not exactly the correct value because the real indenter angle is not specified. However, if the contact area is recalculated by Eqs. (6) and (7) using f_V in the newly obtained contact-depth function, the final contact area for Vickers hardness is correct. To identify this imaginary f_V and constant contact-depth function (a, b), we substitute them into f'_V, a', and b'. The derivation procedure for the contact-depth function and Vickers hardness of an unknown indenter is summarized in Fig. 7.

5. Conclusions

A modified scaling relation taking into account real contact depth including material pileup was suggested. By analysis of the loading–unloading curve, we obtained a contact-depth function as a function of the indenter angle, plastic constraint factor and indentation depth ratio (maximum and final indentation depth). We found a linear relationship between contact-depth function and the indentation depth ratio when the maximum indentation depth and plastic constraint factor are constant. We investigated the effects on the contact-depth function of sharp indenters with different angles. The results show good agreement with our theoretical analysis, and demonstrate that the linear relation is valid for various indenter angles. For practical evaluation of Vickers hardness, we suggested usage of standard hardness blocks to identify the contact-depth equation instead of direct measurement of contact area.

Acknowledgments

This work was supported by the Global Frontier R&D Program (2013-073298) on Center for Hybrid Interface Materials (HIM) funded by the Ministry of Science, ICT & Future Planning, by the Converging Research Center Program through the Ministry of Science, ICT and Future Planning (2013K000411), by the KIST-UNIST partnership program (2.130400.01), and by Basic Science Research Program through the National Research Foundation of

Korea (NRF) funded by the Ministry of Science, ICT & Future Planning (2012R1A1A1043463).

References

[1] Johnson KL. Contact mechanics. Cambridge: Cambridge University Press; 1985.
[2] Cheng YT, Cheng CM. Relationships between hardness, elastic modulus, and the work of indentation. Appl Phys Lett 1998;73:614–6.
[3] Cheng YT, Cheng CM. What is indentation hardness? Surf Coat Technol 2000;417:133–4.
[4] Alcala J, Barone AC, Anglada M. The influence of plastic hardening on surface deformation modes around Vickers and spherical indents. Acta Mater 2000;48:3451–64.
[5] Choi Y, Lee HS, Kwon D. Analysis of sharp-tip-indentation load–depth curve for contact area determination taking into account pile-up and sink-in effects. J Mater Res 2004;19:3307–15.
[6] Kim SH, Lee BW, Choi Y, Kwon D. Quantitative determination of contact depth during spherical indentation of metallic materials—a FEM study. Mater Sci Eng A 2006;415:59–65.
[7] Jeon EC, Kim JY, Baik MK, Kim SH, Park JS, Kwon D. Optimum definition of true strain beneath a spherical indenter for deriving indentation flow curves. Mater Sci Eng A 2006;419:196–201.
[8] Malzbendera J, de With G. Indentation load–displacement curve, plastic deformation, and energy. J Mater Res 2002;17:502–11.
[9] McElhaney KW, Vlassak JJ, Nix WD. Determination of indenter tip geometry and indentation contact area for depth-sensing indentation experiments. J Mater Res 1998;13:1300–6.
[10] Mencik J, Swain MV. Error associated with depth sensing micro-indentation. J Mater Res 1995;10:1491–501.
[11] Lee YH, Hahn JH, Nahm SH, Jang JI, Kwon D. Investigations on indentation size effects using a pile-up corrected. J Phys D: Appl Phys 2008;41(7):074027.
[12] Bolshakov A, Pharr GM. Influences of pileup on the measurement of mechanical properties by load and depth-sensing. J Mater Res 1998;13(4):1049–58.
[13] Chicot D, de Baets P, Staia MH, Puchi-Cabrera ES, Louis G, Perez Delgado Y, Vleugels J. Influence of tip defect and indenter shape on the mechanical properties determination by indentation of a TiB_2–60%B_4C ceramic composite. Int J Refract Met Hard Mater 2013;38:102–10.
[14] Cheng YT, Cheng CM. Scaling, dimensional analysis, and indentation measurements. Mater Sci Eng R 2004;44:91–149.
[15] Cheng YT, Cheng CM. Scaling relationships in conical indentation of elastic perfectly plastic solids. Int J Solids Struct 1999;36:1231–43.
[16] Kang SK, Kim JY, Park CP, Kim HU, Kwon D. Conventional Vickers and true instrumented indentation hardness determined by instrumented indentation tests. J Mater Res 2010;25:337–43.
[17] Kang SK, Kim JH, Lee YH, Kim JY, Kwon D. Correlation between the plastic strain and the plastic pileup of the instrumented indentation by utilizing the interrupted tensile test. Mater Sci Eng A 2012;535:197–201.
[18] Doerner MF, Nix WD. A method for interpreting the data from depth-sensing indentation instruments. J Mater Res 1996;1:601–9.
[19] Oliver WC, Pharr GM. An improved technique for determining hardness and elastic-modulus using load and displacement sensing indentation experiments. J Mater Res 1992;7:1564–83.
[20] Fischer-Cripps AC. A review of analysis methods for submicron indentation testing. Vacuum 2000;58:569–85.
[21] Oliver WC, Pharr GM. Measurement of hardness and elastic modulus by instrumented indentation: advances in understanding and refinements to methodology. J Mater Res 2004;19:3–20.
[22] ISO Metallic materials — Instrumented indentation test for hardness and materials parameters; Part 1 Test method, ISO 14577-1, International Organization for Standardization, Geneva, Switzerland, 2002.
[23] Kim H-U. Determination of contact area for Vickers indentation considering elastic recovery & pile up effect in instrumented indentation technique [Ph.D. thesis]. Korea: Seoul National University; 2009.
[24] ISO Metallic materials — Vickers hardness test — Part 2: verification and calibration of testing machines, ISO 6507-2, International Organization for Standardization, Geneva, Switzerland, 2007.